FULL PAPER

Properties of Flame Sprayed $Ce_{0.8}Gd_{0.2}O_{1.9-\delta}$ Electrolyte Thin Films

Nikolaos I. Karageorgakis, Andre Heel, Jennifer L. M. Rupp, Myriam H. Aguirre, Thomas Graule, and Ludwig J. Gauckler**

Thin films of $Ce_{0.8}Gd_{0.2}O_{1.9-\delta}$ (CGO) are deposited by flame spray deposition with a deposition rate of about 30 nm min^{-1}. The films (deposited at 200 °C) are dense, smooth, and particle-free and show a biphasic amorphous/nanocrystalline microstructure. Isothermal grain growth and microstrain are determined as a function of dwell time and temperature and correlated to the electrical conductivity. CGO films annealed for 10 h at 600 °C present the best electrical conductivity of 0.46 S m^{-1} measured at 550 °C. Reasons for the superior performance of films annealed at low temperature over higher-temperature-treated samples are discussed and include grain-size evolution, microstrain relaxation, and chemical decomposition. Nanoindentation measurements are conducted on the CGO thin films as a function of annealing temperature to determine the hardness and elastic modulus of the films for potential application as free-standing electrolyte membranes in low-temperature micro-SOFCs (solid oxide fuel cells).

1. Introduction

Thin films of ceria (CeO_2) and ceria solid solutions such as $Ce_{1-x}Gd_xO_{2-\delta}$ find use in many applications such as catalysis,[1] electrochromic windows,[2] gas sensors,[3] dielectric layers,[4] insulating layers between superconductors and semiconductors,[5] and as electrolytes in solid oxide fuel cells (SOFC),[6] especially in combination with iron and cobalt containing perovskite cathodes. Micro-SOFCs are novel electrochemical devices operating below 500 °C, with potential application in portable electronics.[7,8] These devices require thin film technology to reduce the internal ohmic losses. They may be integrated as free-standing membranes on micro-machinable substrates, e.g., on Si-single crystals[9] or Foturan glass ceramic.[10]

Many techniques can be used to deposit ceria thin films.[11] Spray pyrolysis is a rather simple and inexpensive method, and does not use vacuum during film deposition.[6] However, in spray pyrolysis the deposited films contain organic residues and residual OH groups from the solvents and require post deposition annealing in order to heal out these defects.[12]

Besides spray pyrolysis, also spin coating,[13] pulsed lased deposition,[14] radio frequency sputtering,[15] physical vapor deposition,[16] and sol-gel methods[17] have been employed for the deposition of ceria-based thin films.

Among these thin film deposition techniques, flame spray deposition reveals a new wet-chemistry based technique where deposition is processed in air. In contrast to previous work about combustion chemical vapor deposition of CeO_2 thin films by Carter et.al.,[18] who worked at rather high deposition temperatures of 1000 °C, we have recently reported the details of the flame spray deposition process for dense CGO thin films[19] at temperatures as low as 200 °C. The benefits of this method are the very high deposition rates of about 30 nm min^{-1} compared to other thin film processes such as PVD, spray pyrolysis and CVD, for which the deposition rates are limited to a few nm min^{-1},[20] the relatively easy scale-up, the use of low-cost precursors and the deposition in air at low deposition temperatures (~200 °C).

The aim of this work is to investigate and correlate the microstructural characteristics of the flame-deposited CGO thin films with the electrical and mechanical properties of the films. Finally, the potential application of flame spray CGO thin films as electrolyte in micro-SOFCs is discussed.

2. Results and Discussions

2.1. Morphology and Microstructure of Flame-Deposited CGO Thin Films

The scanning electron microscopy (SEM) top-view and corresponding cross-section of an as-deposited $Ce_{0.8}Gd_{0.2}O_{1.9-\delta}$ thin film prepared by flame spray deposition with a thickness of

N. I. Karageorgakis, Dr. A. Heel, Prof. T. Graule
Laboratory for High Performance Ceramics, EMPA
Swiss Federal Laboratories for Materials Testing and Research
Ueberlandstrasse 129, Dübendorf, CH-8600, Switzerland
E-mail: nikarageo@gmail.com; ludwig.gauckler@mat.ethz.ch
Dr. J. L. M. Rupp, Prof. L. J. Gauckler
Nonmetallic Inorganic Materials
Department of Materials, ETH Zürich
Wolfgang-Pauli-Str. 10, Zürich, CH-8093, Switzerland
Dr. M. H. Aguirre
Laboratory for Solid State Chemistry and Catalysis, EMPA
Swiss Federal Laboratories for Materials Testing and Research
Ueberlandstrasse 129, Dübendorf, CH-8600, Switzerland

DOI: 10.1002/adfm.201001622

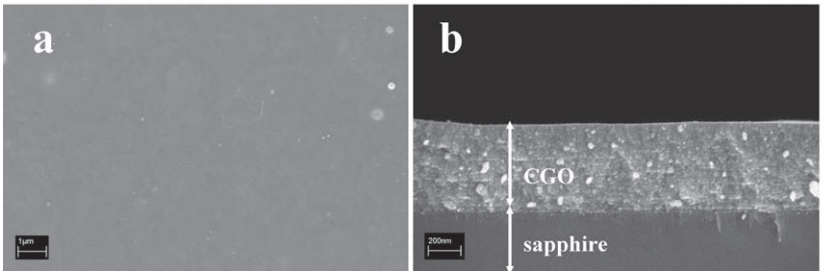

Figure 1. SEM top-view (a) and corresponding cross-section (b) of an as-deposited CGO thin film on sapphire. The film was deposited within 15 min at 200 °C by flame spray deposition.

450 nm is displayed in **Figure 1**. The film was deposited within 15 min at a flame temperature of 200 °C. The as-deposited film has a dense, homogenous and crack-free microstructure. The surface of the film is smooth and particle free. These layers exhibit low surface roughness, in direct contrast to rough and particle-rich layers deposited by other flame-based techniques.[18,21] The as-deposited CGO films have an arithmetic average roughness R_a of 5.1 ± 0.4 nm, as evidenced by AFM measurements in our earlier investigation.[19]

Figure 2 shows the X-ray diffraction (XRD) patterns of an as-deposited CGO thin film, as well as of films annealed for 4 h at various temperatures.

The as-deposited CGO film shows X-ray halos at $2\theta = 27°$, indicating short range order at the position of the (111) reflection in crystalline films, whereas the annealed films exhibit distinct diffraction peaks. The as-deposited films are in amorphous or slightly biphasic amorphous-nanocrystalline state, comparable to the spray pyrolysis deposited films.[12] The amorphous amount gradually decreases through high temperature annealing above 600 °C as indicated by the sharpening of the XRD peaks. The thermodynamic stability of the crystalline films, which results from the lower energy state of the crystalline films compared to the amorphous, is the driving force for

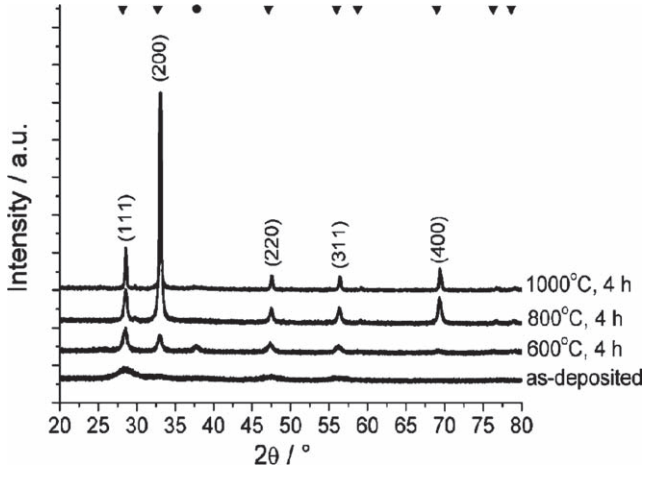

Figure 2. XRD patterns of as-deposited CGO thin film and films after annealing for 4 h at different temperatures. Cubic fluorite structure of $Ce_{0.8}Gd_{0.2}O_{1.9-\delta}$ can be assigned to the films annealed at temperatures above 600°C according to the Joint Committee on Powder Diffraction Standards (JCPDS) database, PDF Card 01–075-0162. Reflections of phase pure CGO are indicated by (▾) and of the sapphire substrate by (●).

crystallization of these films.[12] Reflections corresponding to the cubic fluorite structure of $Ce_{0.8}Gd_{0.2}O_{1.9-\delta}$ (JCPDS database, Card 01–075-0162) are identified. It is interesting to note that during post deposition heat treatments above 600 °C the thin films' texture changes from a (111) dominated to a (200) one. Similar findings were earlier reported for spray pyrolysis CGO thin films[22] and sol–gel[13] thin films of equal chemical composition. This result is surprising as theoretical force-field calculations showed that the (200) surface of CeO_2 is a polar surface and thus is predicted to have a higher surface energy compared to the (111) and (110) oriented planes.[23–26] On the other hand, a large number of experimental studies have been devoted to CeO_2 surfaces and thin films.[27] These experimental observations generally agree on the stability of the (111) surface that develops often. The (200) texture, on the other hand, is theoretically predicted to have a higher energy, although it has also been observed.[28–30] Chen et al.[31] and Kirk et al.[32] have described the effect of growth temperature on the morphology of CeO_2 by the rate of crystallite growth from the peak intensity of a XRD pattern. They showed that the intensity ratio of the (111) plane to the (200) plane increased with temperature, indicating the difference in the activation energy of the growth reaction between planes. However, the latter results were obtained from powder samples. Our results are in agreement with those obtained by S. Gnanarajan and N. Savvides who studied the evolution of texture in CeO_2 thin films.[33] They found for films deposited onto polycrystalline Hastelloy metal substrates by biased magnetron sputtering, the development of preferential (002) texture as the energy of the ions is increased from zero to above 100 eV. Similar findings have been reported by Wang et al.[34] who deposited CeO_2 films on silicon substrates by spray pyrolysis using a salt solution of ethanol–water mixture followed by pyrolysis in flowing air. Furthermore, Cheng et al.[35] found that a bi-axially aligned cube-textured CeO_2 buffer layer with (002) texture could be grown over a wide processing temperature range and especially found the in-plane (002) texture for high temperature annealing. The influence of the precursor solvent on the texture of combustion synthesized ceria films was pointed out earlier.[18] Ce(III) 2-ethylhexanoate precursor yielded ceria films with a (200) preferred orientation on a-plane sapphire substrates, while tetrakis (2,2,6,6-tetramethyl-3,5-heptanedionato)(IV) cerium-based precursors resulted in a (111) preferred orientation deposited at 1000 °C.

At present, there seems to exist no unified opinion among experimentalists and theoreticians concerning the surface energies and preferred surface textures of the (200) and (111) surfaces. Further work is needed to elaborate the texture that develops on CGO and CeO_2 thin film surfaces.

Figure 3 presents the microstructure of the CGO thin films with respect to annealing temperature. Morphology of the CGO films changes by further heat treatment above 800 °C, as documented in Figure 3. The roughness of the films increases, due to the grain growth, reaching a maximum R_a of 38.2 ± 1.2 nm at 1200 °C.[19] However, films remain crack-free and dense independent of the heat treatment.

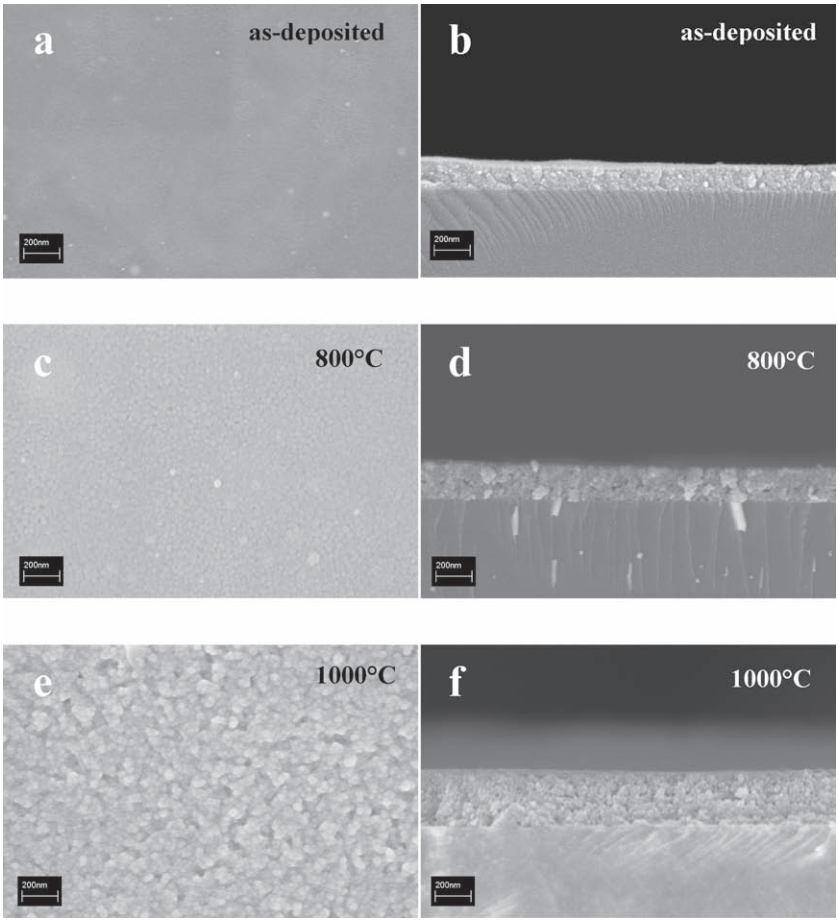

Figure 3. SEM top-views (a,c,e) and corresponding cross-sections (b,d,f) of flame-deposited CGO thin films. Samples presented in (c–f) have been annealed for 4 h. Scale bars: 200 nm.

2.2. Isothermal Grain Growth and Microstrain Evolution During Post Deposition Heat Treatments

The development of grain size and microstrain of the CGO films have been investigated on samples subjected to isothermal dwells at different temperatures. **Figure 4**, presents the grain size evolution over time in the temperature range from 600 °C to 1000 °C.

In the films annealed from 600 °C to 1000 °C the average grain size increases with time. In contrast to normal parabolic grain growth behaviour found in microcrystalline CGO of sintered materials from powder compacts,[36] the grain growth ceases after rather short time of 4–8 h at each temperature, as already observed for CeO_2[12] and CGO thin films prepared by spray pyrolysis.[22] These authors revealed through additional crystallization kinetic studies that this "self-limited grain growth" is driven by transformation of amorphous to fully crystalline phase.[12] Grain sizes of the flame-made CGO films are smaller in comparison to the spray pyrolyzed CGO films and are similar in size to spin coated films from T. Suzuki et al.,[13] always comparing equivalent temperature and time conditions for the post deposition annealing.

The flame spray deposition, under the applied set of parameters, can be characterized as a precipitation-based technique,[19] for which the concentration of introduced defects in the material is higher compared to conventional vacuum-based techniques, like sputtering or pulsed laser deposition,[37] but lower than spray pyrolysis synthesized films.[12,22] In consequence, the relatively high concentration of defects in the flame-made CGO thin films can be the reason for the self-limited grain growth at about 4 h and the resulting smaller grain sizes, compared to materials with less defects from gas phase processes without solvents.

The as deposited and annealed films were also characterized with respect to microstrain that is due to the lattice distortions and the long range displacement fields that extend throughout the grains.[38,39] **Figure 5**, presents the development of microstrain in the CGO films during the isothermal dwells.

During the first 4 h annealing, the microstrain in the CGO films relaxes levelling out at a constant value characteristic for each temperature. Relaxation of microstrain occurs faster at higher temperatures. It is interesting to note, that the microstrain relaxes in similar time spans when the grain growth ceases. Similar relaxation behaviour has also been reported for spray pyrolysis synthesized CGO thin films, where the films needed 10 h of dwell time in order to reach a stable microstructure with fully relaxed microstrain[22] in the same temperature regime. However, the amount of microstrain in the latter work was about one order of magnitude higher, ~7% at 600 °C and 0 h, than the microstrain in the flame-deposited CGO films, ~0.4% at 600 °C and 0 h, of this study. We can conclude that the flame-synthesized films of this study contained less defects

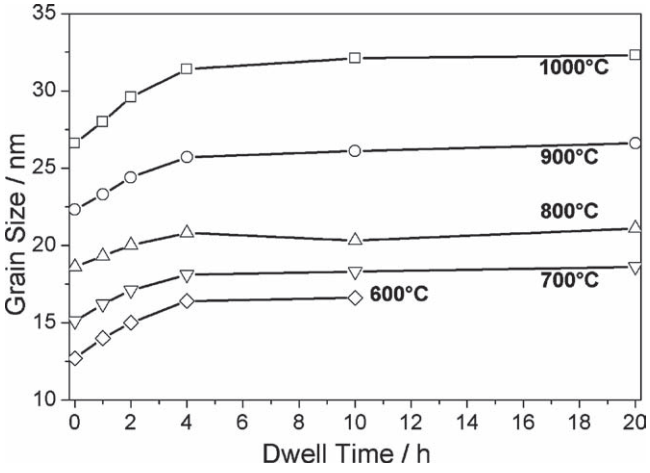

Figure 4. Average grain size during isothermal dwells of flame spray deposited CGO thin films. Error within 10–15%, not shown for clarity.

after deposition than the films derived from spray pyrolysis. This is attributed to the different solvents and precursors used in the film preparation methods and therefore to the corresponding amount of defects and OH impurities incorporated in the films during deposition. Local concentration of strain in nanocrystalline CGO made by plasma sputtering due to point-defects has also been recently reported by Kossoy et al.[40,41]

2.3. Transmissin Electron Microscopy Analysis of CGO Thin Films

Further investigation on the local microstructure of the CGO thin films has been carried out by high-resolution transmission electron microscopy (TEM) on lamellas. Lamellas were taken from CGO samples annealed for 4 h at 800 °C and 1100 °C, respectively by Focused Ion Beam (FIB) tomography. Typical bright field TEM images of films annealed for 4 h at 1100 °C and 800 °C are shown in **Figure 6**a and b, respectively.

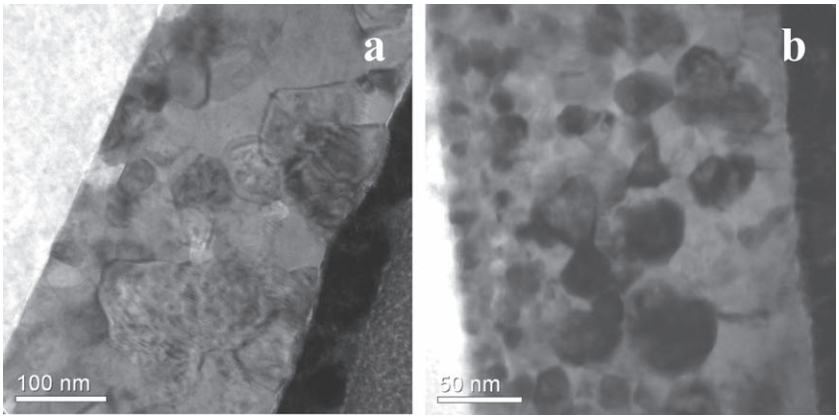

Figure 6. TEM bright field images of CGO lamellas extracted from films annealed for 4 h at (a) 1100 °C and (b) 800 °C, respectively. The bright area on the left of the images is the sapphire substrate and the dark area on the right corresponds to the interface of the CGO film with the sputtered Pt layer, necessary for the FIB preparation of the sample.

In accordance with the SEM investigations, Figure 6 verifies the absence of porosity and documents the dense microstructures of the CGO films. The CGO grain sizes from the TEM confirm the grain sizes calculated from the XRD pattern. An interesting observation here is that a gradient exists in the grain sizes throughout the films. Grains in the proximity of the sapphire substrate (left-hand side) are smaller, and larger grains exist towards the surface of the films (right-hand side).

In **Figure 7**, selected electron diffraction patterns of the two differently annealed samples are shown. Figure 7a represents the sample annealed for 4 h at 1100 °C, where the film is fully crystalline, evidenced by the sharp electron diffraction pattern. The sample annealed at 800 °C shows a diffraction pattern (Figure 7b) with continuous rings and diffuse intensity, due to a possible lower degree of crystallinity and/or smaller grain sizes. Therefore the earlier assumption suggesting that the flame-deposited CGO films annealed for 4 h at 800 °C are either purely amorphous or biphasic amorphous-crystalline is also verified by the electron diffraction in TEM measurements.

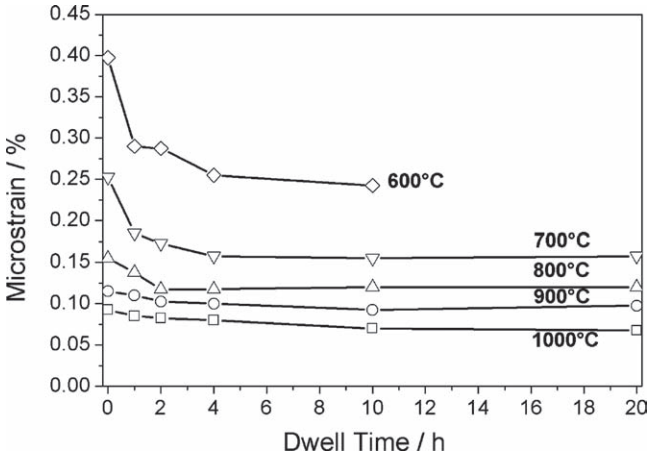

Figure 5. Microstrain evolution of flame-deposited CGO films as a function of annealing temperature and dwell time. Error within 10–15%, not shown for clarity.

Scanning transmission electron microscopy–high angular annular dark field (STEM-HAADF) mode images coupled with EDX line scan have also been used on the CGO lamellas in order to investigate in detail the chemical composition of the grain boundaries and grains of the 1100 °C annealed film. **Figure 8**a shows a STEM-HAADF image of the sample annealed at 1100 °C. This mode shows dark contrast in grain boundaries, due to the lack of heavy elements and bright contrast in some grains, probably owing to large concentration of an element with high atomic mass (excess of Ce). A zoom in a small region, containing the grain boundary is presented in Figure 8b in zero-loss high resolution bright field TEM image. The grain boundary presents bright contrast in between two well crystalline grains and has a thickness of about 2 nm ± 0.2 nm. At the same region, STEM-EDX line scans reveal the composition across the grain boundary: The results are shown in Figure 8c. The EDX line scan shows a constant oxygen concentration in the bulk of the grains and a decrease of oxygen in the grain boundary, coupled with a relatively higher amount of Ce by ~3 at.%, compared to the bulk of the grains. The Gd_L line shows that there is no change in the Gd content throughout the whole line scan across the grain boundary. The same EDX line scans have also been performed across different grain boundaries of the sample and show similar representative results. Therefore, it can be concluded that the grain boundaries in the films annealed at high temperatures are strongly oxygen deficient and may have a different composition from the nominal $Ce_{0.8}Gd_{0.2}O_{2-\delta}$, since the Ce content has been increased in the grain boundary by ~3 at.%. These results are also confirmed in the literature.[42–44]

2.4. Mechanical Characterization of CGO Thin Films

It is essential to characterize the mechanical properties of the CGO thin films used as free standing membranes

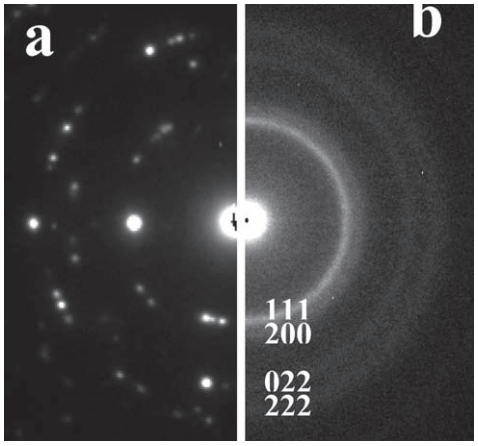

Figure 7. Electron diffraction patterns of CGO films annealed for 4 h at (a) 1100 °C and (b) 800 °C, respectively.

in micro-SOFC applications, in terms of their ability to withstand stresses, which are typically introduced during micromachining.[45] Therefore, nanoindentation measurements have been conducted on CGO films, in order to determine their hardness and elastic modulus, as a function of annealing temperature and isothermal dwell time of 4 h. The most critical mechanical property from the above mentioned is the elastic modulus, since it represents the amount of elastic deformation that the film can withstand without plastically deforming or cracking, which is directly associated with the typical buckling behaviour observed in microfabricated micro-SOFCs.[46] **Figure 9** displays the nanoindentation results as a function of annealing temperature for isothemal dwell time of 4 h.

The as-deposited CGO thin film shows the lowest values for hardness and elastic modulus, due to the biphasic amorphous-nanocrystalline microstructure. This is in agreement with the earlier discussed XRD results. Increasing the annealing temperature results in an increase in hardness and elastic modulus, reaching a maximum between annealing temperature of 800 °C and 900 °C. It can be concluded that the post deposition heat treatment of the films has an influence on their mechanical properties. The soft amorphous matrix of the as-deposited films, in which the nanocrystalline grains are dispersed in an amorphous matrix, has a sufficient structural flexibility and can easily be displaced by the Berkovich tip of the nanoindenter. Therefore the as-deposited film shows the observed low elastic modulus.

Rather low moduli of amorphous materials have also been reported for W-Si-N coatings,[47] where the low hardness and elastic modulus values could be enhanced by post annealing. Nanoindentation measurements have also been performed for alumina films where the amorphous films showed about three times lower hardness and elastic moduli compared to fully crystalline samples.[48] Similar trends for the hardness and elastic modulus has been observed for amorphous and crystalline SiC bulk samples.[49] During post-deposition annealing of the CGO thin films, both, hardness and elastic modulus increase. The grain growth (see also Section 2.2) and the higher degree of crystallinity induced by the annealing temperature result in higher values of hardness and elastic modulus of 11.5 ± 1.4 GPa and 310 ± 43 GPa, respectively, comparable to bulk CGO samples with a hardness of 8.3–9.8 GPa.[50–52] Maximum of hardness and elastic modulus values are reached for the CGO thin films for annealing temperatures between 800 °C and 900 °C. The relatively large error bars, especially for the samples annealed at high temperatures, are due to the increased roughness developing during post heat treatment[19] and the lateral inhomogeneity of the polycrystalline films. Similar behavior, that means enhanced hardness with annealing temperature and grain size, has been reported for Ti-Si-N films by annealing over 1000 °C,[53] for isothermal dwell of Au doped Bi-223 superconductors[54] and CGO bulk samples.[52] Samples annealed at higher temperatures show again lower values for hardness and elastic modulus. This behavior can be explained by the microstructural evolution of the CGO films. By post-deposition annealing above 600 °C, grain growth occurs in parallel to crystallization, where the ratio of crystalline to the initially amorphous phase is constantly increasing, as a function of annealing temperature. It has been reported that fully crystalline ceramic samples

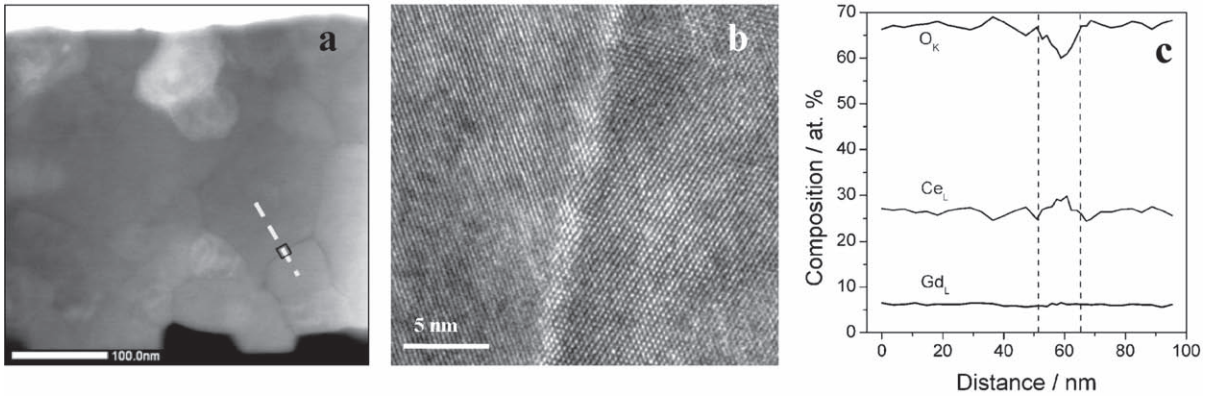

Figure 8. a) STEM-HAADF image of a CGO film annealed for 4 h at 1100 °C. The EDX was taken where the line scan is placed. The square region shows the grain boundary where the most dense point measurements were taken (14 nm–10 points). b) Zero-loss high-resolution bright-field TEM image of the grain boundary investigated by EDX. c) EDX in line scan STEM mode, 0.7 nm electron beam, taken in 3 correlative parts, 1st part: 50 nm–15 points; 2nd: part 14 nm–10 points; 3rd part: 30 nm–10 points with one point overlap. The line scan is shown in (a).

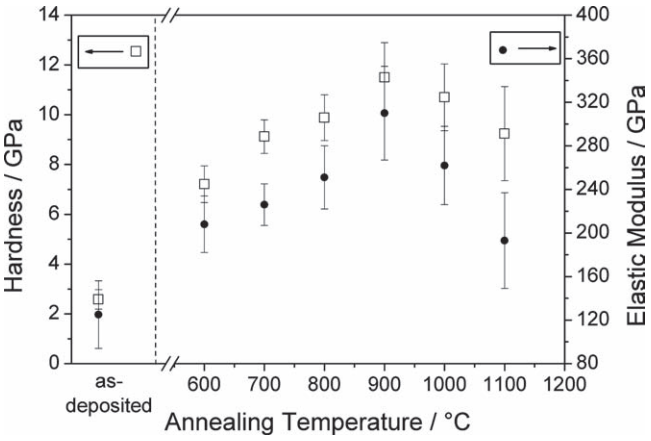

Figure 9. Nanoindentation measurements of CGO thin films annealed at different temperatures and held isothermally for 4 h.

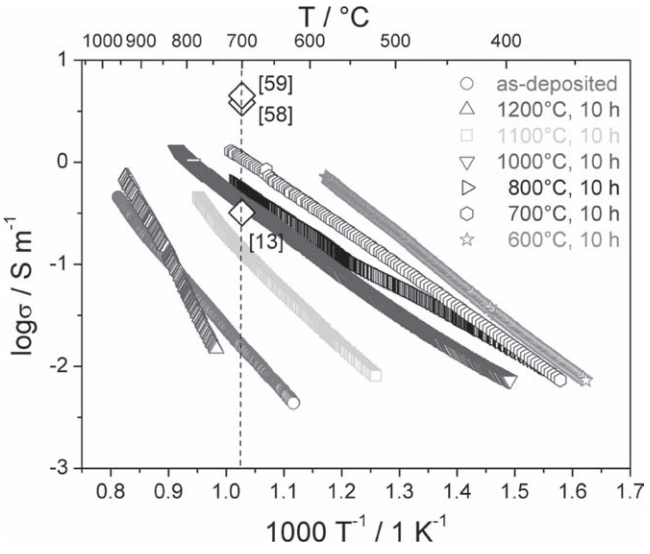

Figure 10. Total electrical conductivity measured in ambient air of flame spray deposited CGO thin films annealed at various temperatures. Dwell time for annealed samples 10 h. Along the dashed line at 700 °C are indicated with (◊) for comparison, conductivity references for: spray pyrolyzed[58] and spin coated[13] CGO thin films as well as bulk CGOc.[59]

have lower hardness values than biphasic amorphous/crystalline ones or nanocomposites of TiN/Si_3N_4 films.[55] This is attributed to the mechanism of deformation in nanocrystalline materials, which is the grain boundary sliding. Fully crystalline materials have no amorphous phase and therefore are brittle. On the other hand, nanocomposites or materials with both nanocrystalline and amorphous phases can elastically deform, due to the propagation of the dislocations and sliding of the grain boundaries in the amorphous phase.[56] Therefore in the CGO thin films prepared by flame spray deposition, it can be concluded that between 800 °C and 900 °C the CGO thin films are mainly nanocrystalline, but still contain some amorphous phase, which is supported by the TEM electron diffraction pattern in Figure 7. At temperatures above 900 °C, the films seem to be fully crystalline and the applied deformation can only propagate by creating micro-cracks, due to the absence of amorphous phase. Therefore a drop in the mechanical properties is observed. Similar correlations of the microstructural features with the mechanical properties has been reported for Ti-Si-N films, where super-hardening results from the combination of amorphous Si and nanocrystalline TiN.[53]

In **Table 1** a comparison can be made between the CGO films prepared in this study and state-of-the-art YSZ films for electrolyte applications in micro-SOFCs. The hardness and elastic moduli reported for flame-deposited YSZ thin films are higher (Table 1). This needs to be taken into consideration during the microfabrication steps of the micro-SOFC.

Table 1. Comparison between mechanical properties of YSZ and CGO samples.

Material	Hardness [GPa]	Elastic Modulus [GPa]	Process
$Ce_{0.8}Gd_{0.2}O_{2-\delta}$ thin film	11.5 ± 1.4	310 ± 43	Flame spray deposition (this work)
$Y_{0.09}Zr_{0.91}O_{2-\delta}$ thin film	16.1 ± 4.6	388 ± 89	Combustion CVD[57]
$Ce_{0.8}Gd_{0.2}O_{2-\delta}$ bulk	9.2 ± 0.2	205	Solid state synthesis[50]
$Ce_{0.8}Gd_{0.2}O_{2-\delta}$ bulk	9.8 ± 0.1	no reference	Homogenous precipitation method[52]
$Ce_{0.9}Gd_{0.1}O_{1.95}$ bulk	8.8 ± 0.2	no reference	Nitrate-fuel combustion[51]
$Y_{0.19}Zr_{0.81}O_{2-\delta}$ bulk	19 ± 0.2	309 ± 6	Single crystal[57]

2.5. Electrical Characterization of Cgo Thin Films

Electrical performance of CGO thin films has been characterized by four point DC conductivity in ambient air, as presented in an Arrhenius plot of the logarithm of total conductivity versus T^{-1} for various annealing temperatures in **Figure 10**.

It is observed for the flame-deposited CGO films that conductivity decreases with increasing annealing temperature. This trend has also been reported for CGO thin films prepared by other deposition techniques, such as spray pyrolysis,[58] pulsed laser deposition,[58] and spin coating.[13] The highest conductivity for CGO thin films is reported for samples annealed for 10 h at 600 °C with a conductivity of 0.46 S m^{-1} at 550 °C. This value is comparable to the conductivity of 0.44 S m^{-1} at 550 °C, reported by the sprayed pyrolyzed CGO thin films annealed at 800 °C for 10 h.[58] Comparing samples annealed isothermally for 10 h of dwell time at 800 °C, flame-deposited CGO thin films show 0.58 S m^{-1}, spin coated films 0.32 S m^{-1} and spray pyrolyzed films 3.83 S m^{-1} at 700 °C, respectively. The flame-deposited CGO thin films show lower conductivity values compared to bulk CGO samples that have 2.8–4.8 S m^{-1} at 700 °C,[59] in agreement with results presented by other groups.[13,58] **Figure 11** depicts the activation energy for the total conductivity of the flame-deposited CGO films, derived from the slope in the Arrhenius plot and the conductivity values measured at 550 °C, as a function of the annealing temperature of the films.

The reported activation energies of this work are higher than the bulk CGO microcrystalline pellets that show 0.71 eV, but

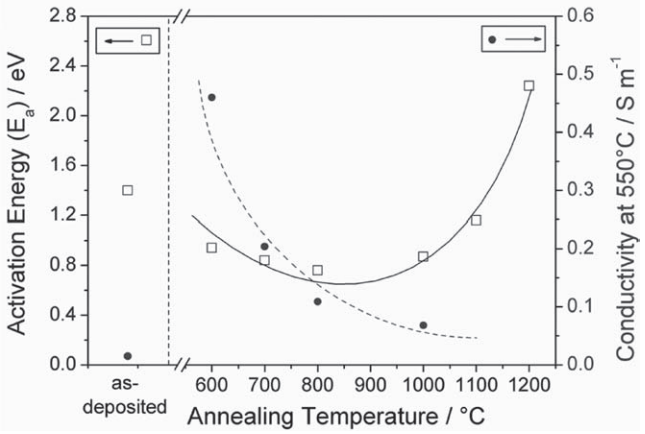

Figure 11. Activation Energies (E_a) of CGO films annealed at various temperatures (left-hand *y*-axis) and corresponding total conductivity values at 550 °C of operating temperature (right-hand *y*-axis). Dwell time for annealed samples 10 h. Error within 10%, not plotted for clarity.

they are in a good agreement with CGO thin films prepared by spin coating,[13] pulsed laser deposition,[58] and spray pyrolysis.[58] It can be clearly seen that the as-deposited CGO films by flame spray deposition show a high activation energy and a low conductivity. This can be explained by the high degree of disorder in these films that limits the mobility of the oxygen ions and therefore a high energy is required to activate the ionic conductivity mechanism in the as-deposited films.

3. Conclusions

CGO thin films prepared by flame spray deposition have been characterized in terms of microstructure, mechanical properties and electrical performance. The as-deposited CGO thin films at a flame deposition temperature of 200 °C on sapphire substrates are dense, smooth, crack-free and particle-free. The as-deposited films have either an amorphous or slightly biphasic amorphous/nanocrystalline microstructure and require heat treatment for further crystallization. Upon heating they are getting nanocrystalline with grain sizes ranging from 12 nm at 600 °C up to 33 nm at 1000 °C. Isothermal self-limited grain growth and microstrain relaxation have been observed for isothermal heating from 600 °C to 1000 °C. Furthermore, TEM investigations have revealed strong oxygen deficiency and some cerium excess in the grain boundaries for samples annealed at high temperature of 1100 °C, suggesting a less-conducting phase composition. The hardness and elastic modulus of the CGO films have been investigated as a function of annealing temperature, for their application as free standing electrolyte membranes in low temperature micro-SOFCs. Annealing temperatures of 800–900 °C yield the best mechanical performance of 11.5 ± 1.4 GPa for hardness and 310 ± 43 GPa for elastic modulus. Electrical conductivity has also been investigated for samples annealed at different temperatures, resulting in highest total conductivity for CGO films annealed at 600 °C for 10 h. The electrical conductivity of the films has been found to decrease with increasing annealing temperature, microstrain and decreasing grain size. For the application of the micro-SOFCs, CGO thin films annealed at 800 °C should be chosen as electrolyte layers to ensure a high mechanical stability and a reasonable electrical performance.

4. Experimental Section

Thin-Film Preparation: The $Ce_{0.8}Gd_{0.2}O_{1.9-\delta}$ (CGO) thin films have been prepared by flame spray deposition. In this technique a liquid solution is prepared by mixing suitable precursors and is fed by a syringe pump into the flame. The experimental setup has been described in detail elsewhere.[19] The flame is created by igniting a mixture of CH_4 (2 L min^{-1}) and O_2 (7 L min^{-1}). The precursor solution consisted of cerium nitrate ($Ce(NO_3)_3{\cdot}6H_2O$, Sigma–Aldrich, 99% purity) and gadolinium nitrate ($Gd(NO_3)_3{\cdot}6H_2O$, Sigma–Aldrich, 99% purity) dissolved in *N*,*N*-dimethylformamide (DMF) (Fluka, 98% purity). This solution (total metal concentration of 0.006 mol L^{-1}) is fed through a capillary to be atomized by dispersion O_2 (20 L min^{-1}) into the hot zone of the flame. The deposition temperature (200 °C) has been monitored by positioning a thermocouple (accuracy ±10 °C) at the back of the sapphire substrate (Stettler, Switzerland).

Characterization Techniques: The morphology of the as-deposited CGO thin films as well as the samples annealed at different temperatures was characterized by scanning electron microscopy (SEM, LEO 1530, Germany). Microstructural features such as grain size and microstrain were calculated using the data obtained from X-ray diffraction measurements (XRD, Siemens S5000, Germany). XRD was performed using Bragg-Brentano configuration from 20° to 80° with step size of 0.009° and scan time of 3 s step^{-1}. The broadening of the peaks (full width at half maximum, FWHM) obtained from the XRD measurements consist of the microstructural characteristics of the film (grain size, microstrain) and a contribution due to instrumental broadening.[60] Instrumental broadening was taken into account by using the Warren–Biscoe equation.[61] Grain size and microstrain were calculated by the intercept in the *y*-axis and the slope, of the linear relation between FWHM·cosθ and sinθ, obtained from the Williamson–Hall plot.[62] Hardness and elastic modulus have been calculated by nanoindentation measurements (Nanoindenter XP, MTS, Oak Ridge TN, USA) using the Oliver–Pharr algorithm.[63] Some considerations included in the nanoindentation measurements are the following: Nanoindentation of a soft material (like CGO) on a hard substrate (like sapphire) should not be influenced by the substrate throughout the whole thickness of the film,[64] but to ensure trustful results the indentation depth was limited to about 10% of the film thickness.[65] Furthermore, a single nanoindentation measurement (load-displacement curve) provides information on elastic deformation only locally,[64] due to the polycrystalline microstructure of the CGO films. Therefore several single load-displacement curves (about twenty) with a load of 1 mN were obtained and the average value of hardness and elastic modulus were calculated. Nanoindentation experiments were performed at different regions of the samples' surfaces to avoid surface effects in the case of neighbouring indentations. Furthermore, low roughness values are required for determining with high accuracy values of hardness and elastic modulus.[64,66] Electrical characterization was performed by in-plane four-point DC conductivity measurements in ambient air, using similar configuration with.[58] Finally two lamellas have been extracted by Focused Ion Beam (FIB) tomography from two CGO films annealed at 800 °C and 1100 °C respectively. The electron column of the FIB device (DualBeam FIB-SEM, Strata DB 235, FEI) was equipped with a field emission gun and through-the-lens detectors (TLD). The lamellas extracted from the FIB tomography were investigated by transmission electron microscopy (TEM). For that purpose, a Jeol JEM FS2200 was used in transmission and scanning mode (STEM). High angular annular dark field (HAADF) images were taken in scanning mode with 0.7 nm spot size beam as well as EDX line scan through the grain boundaries. The Jeol microscope was coupled with a 50 mm^2 window EDX detector and JED-2200 software analysis station.

Acknowledgements

Financial support from the Competence Centre for Materials Science and Technology (CCMX) for funding the NANCER project is gratefully acknowledged. We also wish to thank Dr. Patrick Schwaller, EMPA Thun, for the nanoindentation measurements.

Received: August 4, 2010
Published online: December 10, 2010

[1] T. Skala, F. Sutara, M. Cabala, M. Skoda, K. C. Prince, V. Matolın, *Appl. Surf. Sci.* **2008**, *254*, 6860.
[2] F. E. Ghodsia, F. Z. Tepehana, G. G. Tepehan, *Sol. Energy Mater. Sol. Cells* **2008**, *92*, 234.
[3] N. Wakiya, Y. Kimura, N. Sakamoto, D. Fu, T. Hara, T. Ishiguro, T. Kiguchi, K. Shinozaki, H. Suzuki, *J. Ceram. Soc. Jpn.* **2009**, *117*, 1004.
[4] M. Suzuki, T. Ami, *Mater. Sci. Eng. B* **1996**, *41*, 166.
[5] J. Qiao, C. Y. Yang, *Mater. Sci. Eng. R* **1995**, *14*, 157.
[6] D. Perednis, L. J. Gauckler, *Solid State Ionics* **2004**, *166*, 229.
[7] A. Bieberle-Hutter, D. Beckel, A. Infortuna, U. P. Muecke, J. L. M. Rupp, L. J. Gauckler, S. Rey-Mermet, P. Muralt, N. R. Bieri, N. Hotz, M. J. Stutz, D. Poulikakos, P. Heeb, P. Muller, A. Bernard, R. Gmur, T. Hocker, *J. Power Sources* **2008**, *177*, 123
[8] A. Evans, A. Bieberle-Hutter, J. L. M. Rupp, L. J. Gauckler, *J. Power Sources* **2009**, *194*, 119.
[9] J. H. Shim, C.-C. Chao, H. Huang, F. B. Prinz, *Chem. Mate.* **2007**, *19*, 3850.
[10] U. P. Muecke, D. Beckel, A. Bernard, A. Bieberle-Hutter, S. Graf, A. Infortuna, P. Muller, J. L. M. Rupp, J. Schneider, L. J. Gauckler, *Adv. Funct. Mate.* **2008**, *18*, 3158.
[11] J. Will, A. Mitterdorfer, C. Kleinlogel, D. Perednis, L. J. Gauckler, *Solid State Ionics* **2000**, *131*, 79.
[12] J. L. M. Rupp, B. Scherrer, A. S. Harvey, L. J. Gauckler, *Adv. Funct. Mater.* **2009**, *19*, 1.
[13] T. Suzuki, I. Kosacki, H. U. Anderson, *Solid State Ionics* **2002**, *151*, 111.
[14] L. G. Coccia, G. C. Tyrrell, J. A. Kilner, D. Waller, R. J. Chater, I. W. Boyd, *Appl. Surf. Sci.* **1996**, *96–98*, 795.
[15] G. Chiodelli, L. Malavasi, V. Massarotti, P. Mustarelli, E. Quartarone, *Solid State Ionics* **2005**, *176*, 1505.
[16] N. Jordan, W. Assenmacher, S. Uhlenbruck, V. A. C. Haanappel, H. P. Buchkremer, D. Stover, W. Mader, *Solid State Ionics* **2008**, *179*, 919.
[17] Q. Fang, J. Y. Zhang, *Surf. Coat. Technol.* **2002**, *151–152*, 100.
[18] W. B. Carter, G. W. Book, T. A. Polley, D. W. Stollberg, J. M. Hampikian, *Thin Solid Films* **1999**, *347*, 25.
[19] N. I. Karageorgakis, A. Heel, T. Graule, L. J. Gauckler, *Solid State Ionics* **2010**, doi:10.1016/j.ssi.2010.04.030.
[20] D. Beckel, A. Bieberle-Hutter, A. Harvey, A. Infortuna, U. P. Muecke, M. Prestat, J. L. M. Rupp, L. J. Gauckler, *J. Power Sources* **2007**, *173*, 325.
[21] H. Song, C. Xia, G. Meng, D. Peng, *Thin Solid Films* **2003**, *434*, 244.
[22] J. L. M. Rupp, A. Infortuna, L. J. Gauckler, *Acta Materialia* **2006**, *54*, 1721.
[23] J. C. Conesa, *Surf. Sci.* **1995**, *339*, 337.
[24] S. Vyas, R. W. Grimes, D. H. Gay, A. L. Rohl, *J. Chem. Soc. Faraday Trans.* **1998**, *94*, 427.
[25] M. Baudin, M. Wojcik, K. Hermansson, *Surf. Sci,* **2000**, *468*, 51.
[26] N. V. Skorodumova, M. Baudin, K. Hermansson, *Phys. Rev. B* **2004**, *69*, 075401.
[27] A. Trovarelli, *Catalysis by Ceria and Related Materials*, vol. 2, World Scientific, Singapore **2002**.
[28] S. H. Overbury, D. R. Huntley, D. R. Mullins, K. S. Ailey, P. V. Radulovic, *J. Vac. Sci. Technol. A* **1997**, *15*, 1647.
[29] G. S. Herman, *Phys. Rev. B* **1999**, *59*, 14899.
[30] Y. J. Kim, Y. Gao, G. S. Herman, S. Thevuthasan, W. Jiang, E. McCready, S. A. Chambers, *J. Vac. Sci. Technol. A* **1999**, *17*, 926.
[31] H. Chen, H.-Y. Chang, *Ceram. Int.* **2005**, *31*, 795.
[32] N. B. Kirk, J. V. Wood, *J. Mater. Sci.* **1995**, *30*, 2171.
[33] S. Gnanarajan, N. Savvides, *Thin Solid Films* **1999**, *350*, 124.
[34] S. Wang, W. Wang, Q. Liu, M. Zhang, Y. Qian, *Solid State Ionics* **2000**, *133*, 211.
[35] S. Chen, Z. Sun, K. Shi, S. Wang, J. Meng, Q. Liu, Z. Han, *Physica C* **2004**, *412–414*, 871.
[36] E. Jud, C. B. Huwiler, L. J. Gauckler, *J. Ceram. Soc. Jpn.* **2006**, *114*, 963.
[37] S. Heiroth, T. Lippert, A. Wokaun, M. Döbeli, J. L. M. Rupp, B. Scherrer, L. J. Gauckler, *J. Eur. Ceram. Soc. 30*, 489.
[38] A. Stukowski, J. Markmann, J. Weissmuller, K. Albe, *Acta Materialia* **2009**, *57*, 1648.
[39] A. L. Patterson, *Phys. Rev.* **1939**, *56*, 978.
[40] A. Kossoy, Y. Feldman, R. Korobko, E. Wachtel, I. Lubomirsky, J. Maier, *Adv. Funct. Mater.* **2009**, *19*, 634.
[41] A. Kossoy, Y. Feldman, E. Wachtel, I. Lubomirsky, J. Maier, *Adv. Funct. Mater.* **2007**, *17*, 2393.
[42] J. W. Fergus, *J. Power Sources* **2006**, *162*, 30.
[43] M. Mogensen, N. M. Sammes, G. A. Tompsett, *Solid State Ionics* **2000**, *129*, 63.
[44] H. Inaba, H. Tagawa, *Solid State Ionics* **1996**, *83*, 1.
[45] S. J. Litzelman, J. L. Hertz, W. Jung, H. L. Tuller, *Fuel Cells* **2008**, *5*, 294.
[46] I. Lubomirsky, *Solid State Ionics* **2006**, *177*, 1639.
[47] A. Cavaleiro, A. P. Marques, J. V. Fernandes, N. J. M. Carvalho, J. T. D. Hosson, *J. Mater. Res.* **2005**, *20*, 1356.
[48] G. Alcala, P. Skeldon, G. E. Thompson, A. B. Mann, H. Habazaki, K. Shimizu, *Nanotechnology* **2002**, *13*, 451.
[49] I. Szlufarska, R. K. Kalia, A. Nakano, P. Vashishta, *Appl. Phys. Lett.* **2005**, *86*, 021915.
[50] T. Zhang, Z. Zeng, H. Huang, P. Hing, J. Kilner, *Mater. Lett.* **2002**, *57*, 124.
[51] R. V. Mangalaraja, S. Ananthakumar, K. Uma, R. M. Jimenez, M. Lopez, C. P. Camurri, *Mater. Sci. Eng. A* **2009**, *517*, 91.
[52] T. S. Zhang, J. Ma, L. B. Kong, P. Hing, J. A. Kilner, *Solid State Ionics* **2004**, *167*, 191.
[53] D. Ma, S. Ma, K. Xu, *Surf. Coat. Technol.* **2004**, *184*, 182.
[54] M. Yilmazlar, O. Ozturk, O. Gorur, I. Belenli, C. Terzioglu, *Supercond. Sci. Technol.* **2007**, *20*, 365.
[55] S. Veprek, S. Reiprich, *Thin Solid Films* **1995**, *268*, 64.
[56] H. Watanabe, Y. Sato, C. Nie, A. Ando, S. Ohtani, N. Iwamoto, *Surf. Coat. Technol.* **2003**, *169–170*, 452.
[57] D. W. Stollberg, J. M. Hampikian, L. Riester, W. B. Carter, *Mater. Eng. A* **2003**, *359*, 112.
[58] J. L. M. Rupp, L. J. Gauckler, *Solid State Ionics* **2006**, *177*, 2513.
[59] C. Kleinlogel, L. J. Gauckler, *Solid State Ionics* **2000**, *135*, 567.
[60] S. P. Sengupta, M. De, *Appl. Phys.* **1971**, *4*, 1063.
[61] C. N. J. Wagner, E. N. Aqua, *J. Less-Common Mater.* **1965**, *8*, 51.
[62] G. K. Williamson, W. H. Hall, *Acta Metallurgica* **1953**, *1*, 22.
[63] W. C. Oliver, G. M. Pharr, *J. Mater. Res.* **1992**, *7*, 1564.
[64] P. Schwaller, F. Haug, J. Michler, J. Patscheider, *Adv. Eng. Mater.* **2005**, *7*, 318.
[65] B. Jonsson, S. Hogmark, *Thin Solid Films* **1984**, *114*, 257.
[66] D. W. Stollberg, W. B. Carter, J. M. Hampikian, *Thin Solid Films* **2005**, *483*, 211.